PHYSICAL CONDITIONS IN NEARBY MOLECULAR CLOUDS

PHILIP C. MYERS
Harvard-Smithsonian Center for Astrophysics
60 Garden St.
Cambridge, MA 02138
USA

1. Introduction

In this chapter we describe properties of the nearest star-forming complexes, and physical processes which lead to, and are associated with, star formation. We present basic ideas and recent results, primarily from an observational viewpoint, with emphasis on spectroscopy. We present in §2 general properties of molecular clouds, in §3 properties of dense cores, in §4 the role of turbulent cores in forming star clusters, in §5 evidence for inward motion in dense cores, and in §6 some models of inward motion.

2. Nearby Molecular Clouds

Astronomers call a "molecular cloud" an object which can be detected and mapped in its brightest line, the $J = 1 - 0$ rotational transition of the CO molecule at 2.6 mm wavelength. Molecular clouds are the most massive objects in galaxies, with masses up to more than 10^6 $M_\odot$, and are the birthplaces of stars. They are called "molecular" because their main constituent, hydrogen, is primarily in molecular form, H_2, while their atomic hydrogen component is less abundant by a factor $\sim 10^3$. Because the H_2 molecule has no permanent dipole moment, its emission is much weaker than that of CO, despite the relatively low abundance of CO, $\sim 10^{-4}$.

The nearest molecular clouds, within a few hundred pc of the Sun, are well-studied and well-resolved by molecular line observations. These complexes in Taurus, Ophiuchus, Lupus, Chamaeleon, Perseus, and Orion are evident by their extinction of background starlight, their far infrared emission, and their emission in numerous molecular lines. Many of their features are illustrated in Figure 1, a map of CO emission from the Orion complex

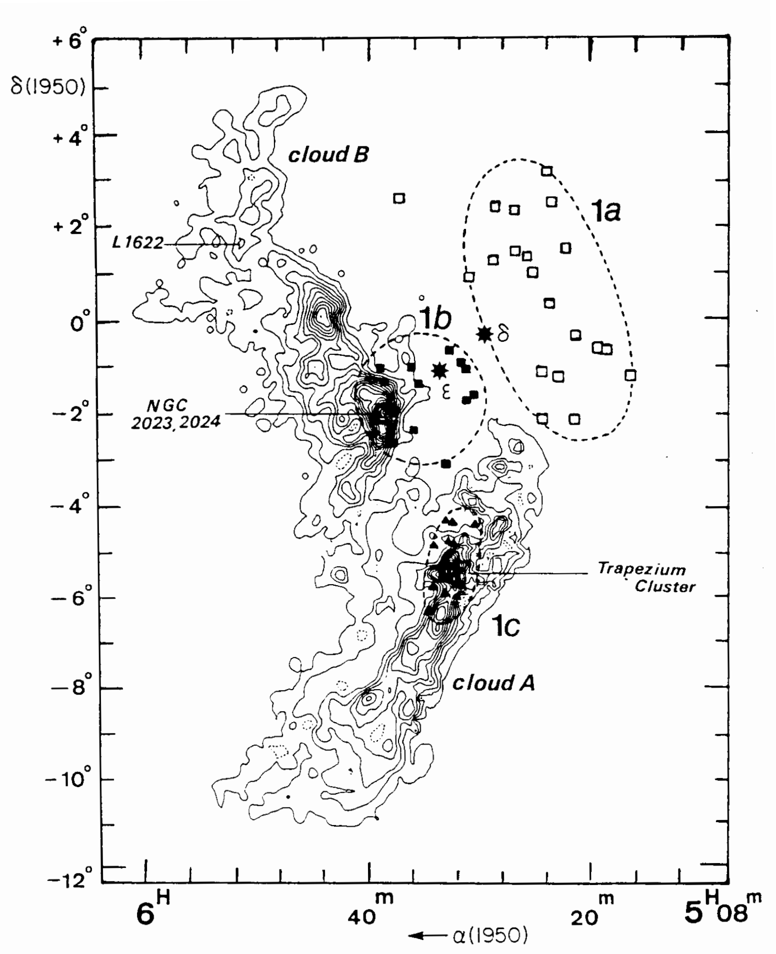

Figure 1. CO line emission from the Orion A and B giant molecular cloud complexes (Maddalena et al 1986), in relation to their associated young star clusters (Blaauw 1991). The overall extent of each complex is about 60 pc.

in relation to its associated star clusters (Blaauw 1991). As revealed by CO line maps, a typical molecular cloud complex has an irregular shape, with "blobs" of low aspect ratio (1-2) and "filaments" of high aspect ratio (5-10). The map as a whole is considered a "complex" because it contains more than one component with closed contours. These components are considered to be physically associated with each other because of their close proximity in projected position and in radial velocity. The individual map structures are called "clouds" or "clumps," and their star forming condensations are known as "cores" or "dense cores."

The overall extent of CO maps of nearby molecular cloud complexes is typically 10-30 pc, and their enclosed mass is 10^{4-6} $M_{\odot}$. The largest regions, called "giant molecular clouds" or "GMCs," have mass exceeding 10^6 $M_{\odot}$, and are the birthplaces of massive stars and rich star clusters. More detailed descriptions of GMCs and of massive star formation are given in the chapters by Blitz and Churchwell, respectively. The Orion complex is the nearest GMC, while the smaller nearby complexes, such as in Taurus and Ophiuchus, are often called "dark clouds" because of their obscuration of background starlight.

The density structure of molecular clouds is highly nonuniform, and its inference from observation requires caution. The mean density depends strongly on the size scale over which the average is taken, and each probe used to map a cloud is sensitive only to a range of density. Thus the mean density over a complex is an average over $\sim$10 pc, or roughly 10^2 cm^{-3}. This density is well sampled by observations of the J=1-0 line of CO. The mean density over a "clump" is an average over $\sim$1 pc, or 10^3 cm^{-3}; this density is traced by the J=1-0 line of ^{13}CO, an isotopomer of ^{12}CO. The mean density over a dense core is an average over $\sim$0.1 pc, or 10^4 cm^{-3}, traced by the (J, K) = (1,1) line of NH_3. This diversity of density implies that no single observable tracer can completely represent the structure of a molecular cloud, regardless of the spatial resolution used: observations of the 1-0 line of CO do not reveal dense cores, and observations of the (1,1) line of NH_3 do not reveal cloud complexes.

2.1. MOLECULAR CLOUD CONSTITUENTS

The main constitutents of molecular clouds are molecules, dust grains, ions, and stars. Here we briefly describe the role each plays in molecular cloud physics.

More than 100 species of interstellar molecules are known, and more than 1000 spectral lines are known at centimeter, millimeter, and submillimeter wavelengths. The simplest molecules are diatomic species such as OH, CH, CO, CS, and their isotopomers. The more complex molecules are carbon chains and rings, and indeed most interstellar molecules are organic species, some of which were first discovered in space and then confirmed by laboratory spectroscopy. The largest interstellar molecule known, as of October 1998, is the carbon chain $HC_{11}N$ (Bell et al 1997), and still longer chains, such as $HC_{17}N$, have been found in the laboratory with sensitive spectroscopic techniques (McCarthy et al 1998). A review of interstellar molecules, and their rich chemistry, is in the chapter by van Dishoeck.

Figure 2 illustrates the variety of molecular lines, observed at a wavelength 0.8 mm in the richest source of bright lines, the Kleinmann-Low nebula in the Orion molecular cloud (Schilke et al 1997). Note that many

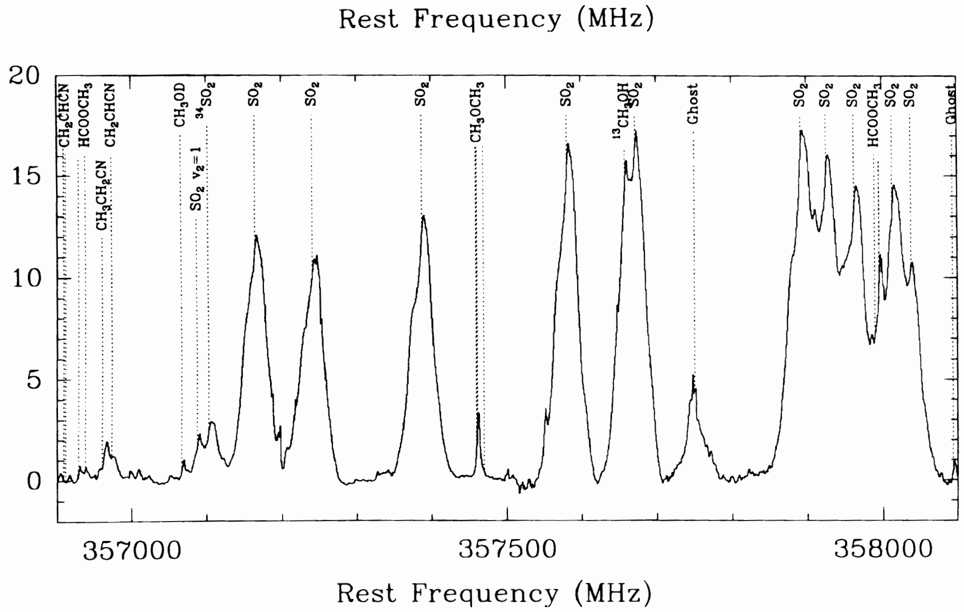

Figure 2. Molecular line emission from the Kleinmann-Low Nebula in Orion, in a spectral window about 1 GHz wide, centered at freqency 357.5 GHz or wavelength 0.84 μm (Schilke et al 1997). Note the high density of lines, and their origin in many complex molecular species.

lines are due to complex organic species, and in some portions of the spectrum there is more flux in lines than between the lines.

The molecular species CO, H_2O, and their isotopomers are especially important because their rotational lines are the main coolants for nearly all of the gas in molecular clouds. This cooling radiation balances the heating, due mainly to cosmic rays and external UV photons, giving an equilibrium temperature of about 10 K. Without these cooling species, molecular clouds would be substantially warmer, approaching the temperatures of diffuse clouds, $\sim$100 K.

Dust grains are solid particles condensed in the atmospheres of giant stars and blown into the interstellar medium by their stellar winds. Dust grains are believed to consist mostly of graphitic carbon and silicates, probably with amorphous, as opposed to crystalline, internal structure. Grains have a typical size of 0.1 μm, and a broad distribution of sizes extending down toward the regime of large molecules. In molecular clouds grains are believed to become the main coolant as the gas density exceeds $\sim 10^5$ cm^{-3}. Grain surfaces are thought to catalyze the formation of H_2 from H. In dense cores grains are expected to have "mantles," layers of molecular material which are deposited as molecules which are sufficiently polar collide with the grain, and bond to the surface. When such grains are heated by radiation from a recently formed star, many of their complex mantle molecules evaporate into the "hot core" gas. Recent reviews of grain properties are in Roberge & Whittet (1996).

Molecular clouds are not entirely neutral, but instead have a low level of ionization, with electron fraction $x_e < 10^{-5}$, due to a combination of cosmic ray ionization and photoionization by ultraviolet photons from distant OB stars. If an OB star forms in the molecular cloud, its UV photons fully ionize the gas in a small portion of the cloud (an "H II region"), while most of the surrounding molecular cloud remains largely neutral. Molecular cloud ionization is important both chemically and physically. Most of the gas-phase chemical reactions in a molecular cloud are driven by ionized species, whose high reaction cross sections make them influential despite their low abundance. Also, the trace ionization in molecular clouds is sufficient to couple, by ion neutral collisions, the motions of the magnetic field to those of the neutral gas. This mechanism allows propagation of magnetohydrodynamic (MHD) waves and turbulence, whereby the magnetic field and the neutral gas move together as a single fluid. These MHD motions are thought to help support molecular clouds against their self-gravity.

Stars are the most interesting and important constituent of molecular clouds. Molecular clouds are believed to be the formation site of all known young stars, and our understanding of how stars form is based on the principle that molecular clouds provide the "intitial conditions" for the process of star birth. Molecular clouds host young stellar objects (YSOs) in a wide range of evolutionary states, from "Class 0 protostars" some 0.01 Myr old, deriving most of their luminosity from gravitational infall, to "T Tauri" stars a few Myr old, deriving their luminosity from quasi-static contraction. Molecular clouds also host stars in a wide range of spatial groupings - from isolated single stars as in Taurus, having no known neighbors within a few pc, to rich star clusters as in Orion, having more than 1000 stars within a few pc. The masses of stars in molecular clouds range from about 0.1 to 30 $M_\odot$, nearly the whole range of known stellar masses. Indeed the initial mass function (IMF), or the distribution of stellar masses at birth, is indistinguishable between stars in molecular clouds and field stars. Reviews of low-mass and massive star formation, from observational and theoretical viewpoints, are given in the chapters by Lada, Churchwell, Shu, and Bonnell.

Embedded stars contribute a major part of the turbulent kinetic energy in molecular clouds, through their winds and outflows. The winds, outflows and radiation from the most massive stars probably limit the lifetime of molecular clouds by unbinding and dispersing their gas.

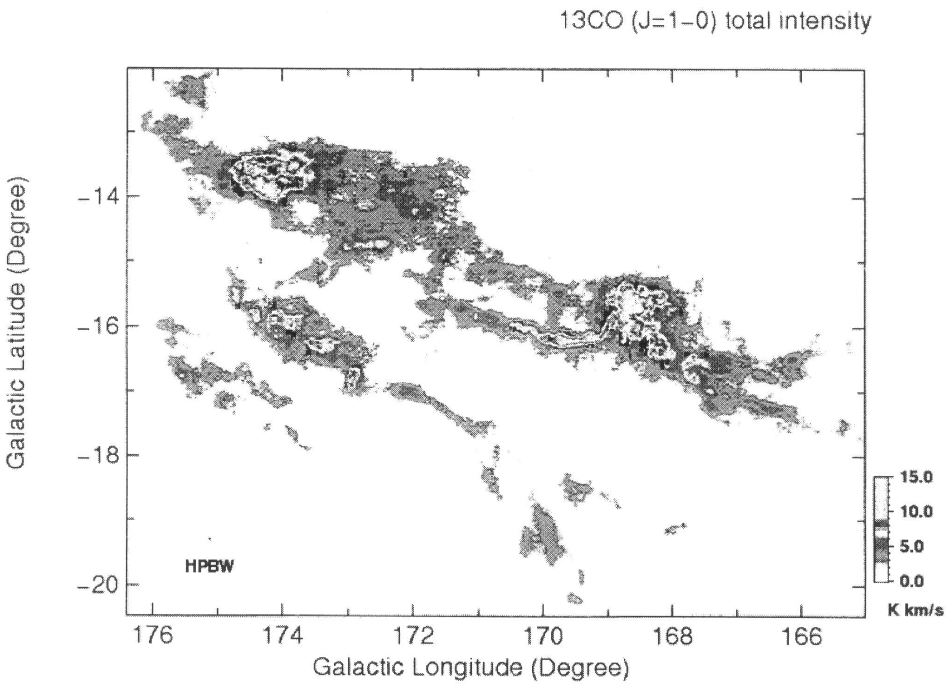

Figure 3. The Taurus molecular cloud complex, in the 2.7 mm wavelength J=1-0 line of ^{13}CO (Mizuno et al 1995). The longest dimension is about 25 pc, substantially less than in Orion (Figure 1). Note the highly elongated, clumpy structure.

2.2. CLOUD DIVERSITY

Molecular clouds differ in numerous ways, and many of their properties vary together with increasing size from region to region (Myers 1991, Harju, Walmsley & Wouterloot 1993, Jijina, Myers & Adams 1998). The smallest molecular cloud complexes, as in Chamaeleon III, have length $\sim$10 pc, maximum visual extinction of a few magnitudes, turbulent line widths of 1 km s^{-1}, temperature 10 K, relatively few stars, no massive stars, and no clusters. The largest complexes, as in Orion, have extent $\sim$50 pc, visual extinction of $\sim$100 magnitudes, turbulent line widths of several km s^{-1}, gas temperature typically 20 K, and thousands of stars in dense clusters, including numerous OB stars. The more massive molecular clouds are responsible for forming most stars, even though the lower-mass clouds are more numerous. Figure 3 shows a map of the Taurus complex in the J=1-0 line of ^{13}CO (Mizuno et al 1995). In relation to other nearby complexes, Taurus is intermediate in its star-forming activity (Chen et al 1995, 1997).

2.3. DENSITY PROBES

Among the hundreds of molecular lines detected in molecular clouds, fewer than ten have been used extensively, because they are relatively bright, because their frequencies are suitable for observation with many telescopes, and because they probe characteristic regimes of density. A spectral line "traces" a particular range of density of hydrogen molecules, which collide with the emitting species and help excite the observed transition. For a simple two-level system in statistical equilibrium, the characteristic density needed for excitation is the "critical density" n_{cr}, at which the rate of spontaneous emission equals the rate of collisional excitation:

$$n_{cr} = \frac{64\pi^4 \mid \mu \mid^2 \nu^3}{3hc^3 < \sigma v >} \tag{1}$$

Here $\mid \mu \mid$ is the transition dipole moment, ν is the transition frequency, h is Planck's constant, c is the speed of light, and $< \sigma v >$ is the collision rate coefficient (Townes & Schawlow 1975; Rohlfs & Wilson 1996). Some representative values of n_{cr} are 10^3 cm^{-3} for the J=1-0 line of CO at 2.6 mm wavelength, 10^4 cm^{-3} for the (J,K) = (1,1) line of NH_3 at 13 mm wavelength, and 10^5 cm^{-3} for the J=2-1 line of CS at 3.0 mm (Ungerechts et al 1997).

If the transition optical depth τ is substantially greater than 1, the critical density in eq. (1) must be modified to account for radiative trapping. In this optically thick case, a molecule has substantial probability of absorbing a transition photon emitted by another molecule in the cloud. Then excitation can occur by both absorption and collisions, and the density needed to achieve a given excitation temperature is reduced. For a plane-parallel cloud and for the "large velocity gradient" approximation to the radiative transfer, n_{cr} in eq. (1) is multiplied by the "trapping factor"

$$\beta = \frac{1 - e^{-3\tau}}{3\tau} \tag{2}$$

(e.g. Rohlfs & Wilson 1996). For the J=1-0 transitions of the isotopomers CO, ^{13}CO, and C^{18}O, the typical critical densities are smaller than in eq. (1) by a factor β^{-1} or 300, 9, and 1.5, respectively. This behavior allows lines of isotopomers to probe different density regimes of the same cloud with essentially the same angular and spectral resolution.

The critical density in eq. (1) is the density at which an optically thin transition has substantial excitation. The degree of excitation is described by the excitation temperature T_{ex}, defined in analogy with the Boltzmann distribution by

$$\frac{n_u}{n_l} = \frac{g_u}{g_l}\exp(-\frac{h\nu}{kT_{ex}}) \tag{3}$$

Here n_u and n_l are the densities of emitting molecules in the transition upper and lower states, respectively, and g_u and g_l are the corresponding statistical weights. To illustrate the role of the critical density, consider the case where the radiation temperature is lower than the kinetic temperature, as shown in Figure 4. This situation arises, for example, when the radiation temperature, $T_R = 2.7$ K, is that of the cosmic microwave background, and the kinetic temperature, $T_k = 10$ K, is due to cooling by CO lines and heating by cosmic rays and UV photons (Goldsmith & Langer 1978). As the gas density decreases below the critical value in eq. (1), the excitation is "subthermal," and the excitation temperature T_{ex} approaches T_R. When the density equals the critical value, T_{ex} is about halfway between T_R and T_k. When the density increases above n_{cr}, the excitation becomes "thermal" and T_{ex} approaches T_k.

The excitation of a transition above its background level is substantial for all densities $n \geq n_{cr}$, but the effective range of density traced by a transition is typically a factor of a few, because the distribution of gas density in molecular clouds decreases rapidly with increasing density. For example, a spherically symmetric cloud having density decreasing with increasing radius as $n \sim r^{-1}$ has differential mass distribution $dm/dn \sim n^{-3}$. Thus observation of a cloud in a particular tracer images the cloud in a limited range of density around n_{cr} – limited at lower densities by the sharp increase of excitation with increasing density, and limited at higher densities by the sharp decrease of cloud mass with increasing density.

3. Dense Cores

We define a "dense core" as a molecular cloud condensation with mean gas density 10^4 cm^{-3}. It is useful to specify 10^4 cm^{-3} as a fiducial density, for several reasons. First, several easily observable molecular lines have effective critical density of order 10^4 cm^{-3}, including the (J, K) = (1,1) line of NH_3 at 1.3 cm and the J=2-1 line of CS at 3.0 mm. These probes have provided a wealth of information about the gas in molecular clouds with density within a factor of a few of 10^4 cm^{-3} (e.g., Linke & Goldsmith 1980; Ho & Townes 1983; Jijina, Myers & Adams 1998). Second, the mass of gas with density 10^4 cm^{-3} in Taurus and other nearby complexes is generally of order 1 $M_\odot$ (Myers & Benson 1983, Benson & Myers 1989). These dense cores have mass comparable to that of the typical low-mass star, and such cores and stars are closely associated, according to observations at far-infrared (Beichman et al 1986) and near-infrared (Myers et al 1987) wavelengths. This association

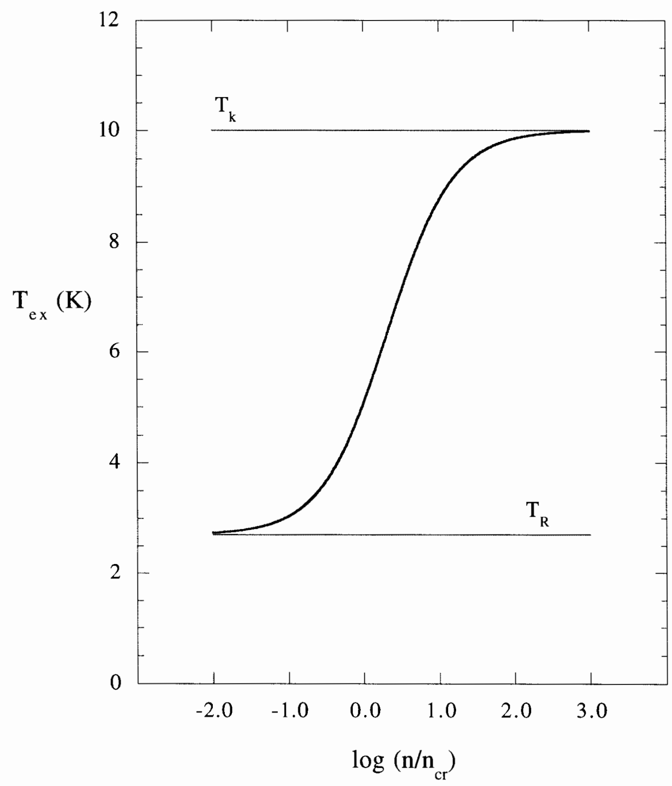

Figure 4. Increase of excitation temperature T_{ex} of a spectral line transition with increasing density n of collision partners. As n increases, T_{ex} increases from its minimum at the radiation temperature T_R to its maximum at the kinetic temperature T_k, reaching appreciable excitation at the critical density n_{cr}.

indicates a close link between the physical properties of the core gas and its evolution to form a star, and provides observational support for models of isolated, low-mass star formation (Shu, Adams & Lizano 1987). Third, maps in lines of CS and NH_3 in regions of more massive star formation tend to be associated with groups and clusters of young stars, suggesting that properties of such cores are related to the formation of groups and clusters (Lada, Bally & Stark 1991; Harju, Walmsley & Wouterlout 1993).

In this section we describe dense core properties as indicated by observations of lines of NH_3, CS, N_2H^+, and HCO^+, which trace densities $\geq 10^4$ cm^{-3}, but not by lines of CO, ^{13}CO, or $C^{18}O$, which trace lower density. First we describe general properties which are independent of the degree of turbulence evident in the line width, and then those which vary with core turbulence.

3.1. STAR FORMATION

In nearby complexes, cores selected by their optical obscuration, without knowledge of their stellar association, have been shown by infrared surveys to have a significant number of associated YSOs (Benson, Myers & Wright 1984, Beichman et al 1986, Myers et al 1987). In Taurus and similar complexes, about half of the 20 cores which have been mapped in NH_3 lines have associated YSOs (Jijina, Myers & Adams 1998, hereafter JMA). Conversely, YSOs with IRAS emission which is sufficiently bright and red, indicating a high column density of cold circumstellar dust, have a high incidence of NH_3 line emission (Harju, Walmsley, & Wouterloot 1991). The association of cores and YSOs is more frequent for redder YSO spectra, supporting the idea that cores are the birth environment of YSOs, and that more evolved YSOs lose their association with their parent cores, probably by a combination of dispersal through outflows (Tafalla & Myers 1997) and relative motion of the core and YSO.

3.2. ELONGATION

Core maps show a significant elongation, with typical aspect ratio of 2, and a clear departure from the circular shape expected for a map of a spherically symmetric system (Benson & Myers 1989, Lada, Bally & Stark 1991, Wood, Myers, & Daugherty 1994). Elongated cores are seen in quiescent, low-mass complexes such as Taurus (Benson & Myers 1989), in intermediate complexes such as Perseus (Ladd, Myers & Goodman 1994), and in massive, turbulent complexes such as Orion (Harju, Walmsley & Wouterlout 1993, Cesaroni & Wilson 1994). Statistics of core map elongation have been interpreted as indicating that most cores have 3-dimensional shape which is prolate, rather than oblate (Myers et al 1991, Ryden 1996). The location of elongated cores in more extended filamentary structures, indicated by their visual extinction and by maps of lower-density tracers, strongly favors the prolate over the oblate interpretation (Myers et al 1991). A detailed discussion of the structure of filamentary clouds is given in Lada (1999). On the other hand, models of core evolution in the context of a relatively strong magnetic field predict oblate structure, with flattening along the direction of the field, and with projected aspect ratio similar to that observed (Lizano & Shu 1989, Basu & Mouschovias 1994, Li & Shu 1996).

Resolution of this apparent discrepancy may require a better understanding of how cores form, and more detailed observations of magnetic field directions in filamentary clouds. For example cores which form from filamentary clouds may have elongated maps because they are prolate, if the magnetic field lies along the filament, or because they are triaxial, if the magnetic field lies perpendicular to the filament. Alternatively, elongated cores may arise if the magnetic field has a helical structure wound around the filamentary parent cloud (Feige & Pudritz 1998).

3.3. VIRIAL BALANCE

Cores have line widths, column densities, and map sizes which appear close to the condition of virial balance, in which the gravitational potential energy and kinetic energy are approximately equal (Myers et al 1991, Harju, Walmsley & Wouterloot 1993). For an isolated uniform sphere of mass M, radius R, and velocity dispersion σ, this condition is

$$\frac{GM}{5R} = \sigma^2 \tag{4}$$

(Spitzer 1978). Figure 5 shows a comparison of dense core data with several virial equilibrium models, indicating that the typical core agrees with most models within the scatter of data, provided that both thermal and nonthermal motions are included. If as usual for molecular clouds virial balance is understood as a statement of approximate hydrostatic equilibrium, then the supporting pressure is $mn\sigma^2$, where σ includes both thermal and nonthermal motions.

The nonthermal motions evident in core line widths span a wide range, from subsonic by a factor $\sim$4 in small quiescent cores such as L1512 (Fuller & Myers 1993) to supersonic by a factor > 10 in large turbulent cores associated with compact H II regions (Ho & Townes 1983). The ratio of nonthermal to thermal motions varies continuously from core to core, but it is convenient to divide cores into "thermal" and "turbulent" regimes, separated by the critical case where the velocity dispersion of the nonthermal motions equals the velocity dispersion of the thermal motions of the molecule of mean mass (Myers, Ladd & Fuller 1991). Here we denote nonthermal motions as "turbulent," without ascribing any particular physical model of turbulence to them. The critical case is easily derived from observations of the (J, K) = (1,1) and (2,2) lines of NH_3 because these observations yield accurate estimates of both the kinetic temperature and the observed line width (Ho & Townes 1983). Denoting the FWHM of the observed line profile, corrected for optical depth and resolution effects, as Δv_{obs}, we may write

$$\Delta {v_{obs}}^2 = \Delta {v_{turb}}^2 + 8\ln 2kT/m_{obs} \tag{5}$$

where Δv_{turb}, the FWHM of the turbulent motions, is independent of mass, and m_{obs} indicates the mass of the observed species. In the critical case $\Delta {v_{turb}}^2 = 8(ln2)kT/m_{obs}$, where m is the mean molecular mass, or $2.3m_H$,

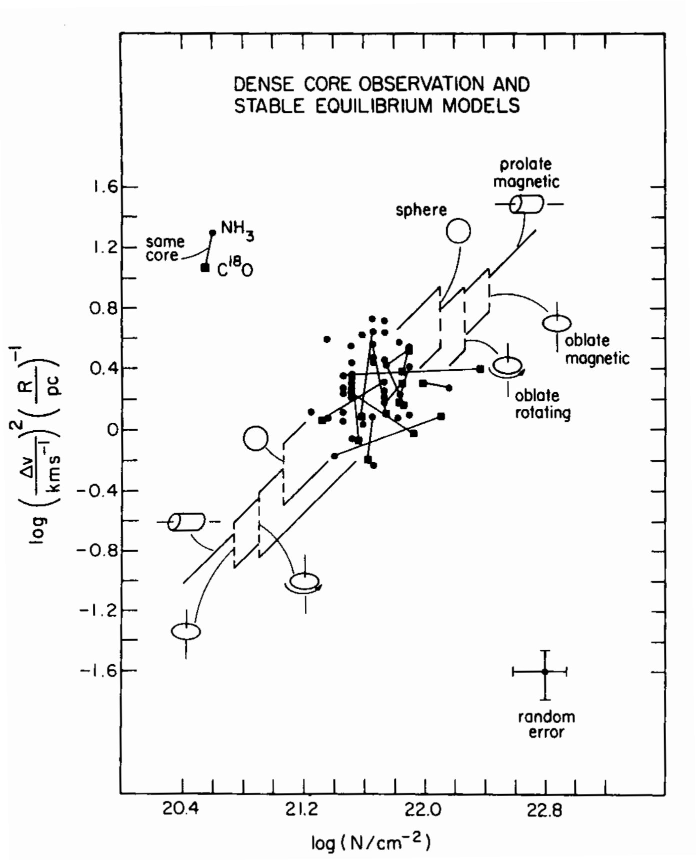

Figure 5. Comparison of dense core line widths, map sizes, and column densities with models of virial equilibrium, based on observations of lines of NH_3 and $C^{18}O$ (Myers et al 1991). The data indicate consistency with most models of core virial equilibrium, although they do not clearly favor any particular model.

assuming one He atom for every five H_2 molecules. Combining this relation with eq. (5) gives the critical line width

$$\Delta v_{obs,cr} = [\frac{8\ln 2kT}{m}(1+\frac{m}{m_{obs}})]^{1/2} \tag{6}$$

For observations of 10 K gas in a line of NH_3, for which $m_{obs} = 17m_H$, the critical line width is 0.47 km s^{-1}.

In the less massive cores, observed NH_3 line widths are less than $\Delta v_{obs,cr}$, so they are thermal, and models of their support against self-gravity can safely ignore their turbulent motions, as in the standard model of isolated star formation (Shu, Adams & Lizano 1987). In the more massive molecular

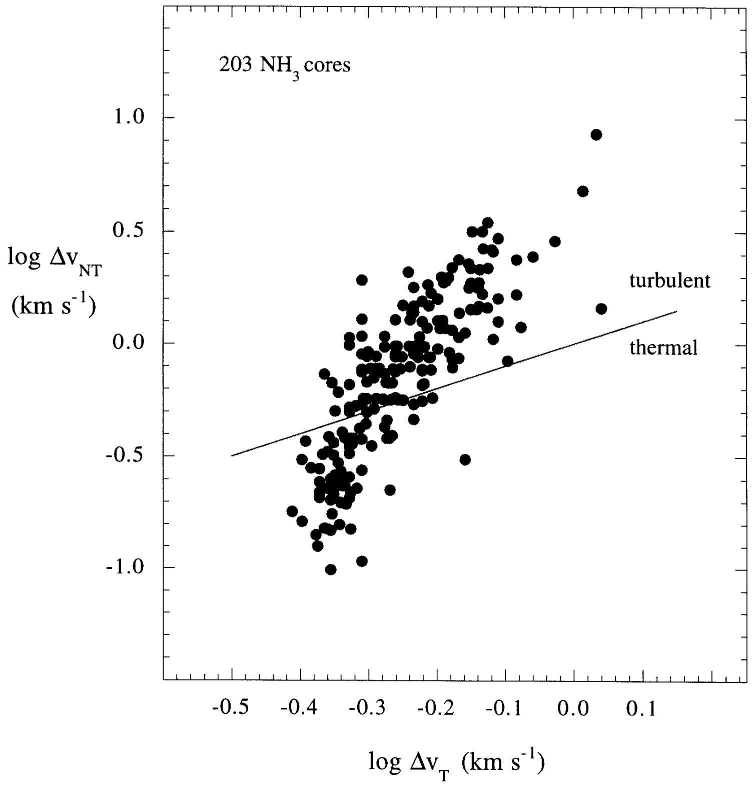

Figure 6. Nonthermal and thermal line widths in NH_3 dense cores. The FWHM of the distribution of nonthermal motions, Δv_{NT}, increases rapidly with the corresponding FWHM of the distribution of thermal motions of the molecule of mean mass, Δv_T. Thus turbulent cores tend to be warm, and quiescent cores tend to be cool (JMA).

cloud cores, observed NH_3 line widths generally exceed $\Delta v_{obs,cr}$, so their turbulent motions exceed their thermal motions. Since these cores approximately satisfy virial balance, eq. (4), their turbulent motions play a key role in supporting them against their self-gravity. Understanding the nature of the turbulent motions remains a major problem in molecular cloud physics.

Figure 6, adapted from JMA, shows that the nonthermal and thermal components of the line width observed in NH_3 cores tend to correlate, so that cores which exceed their critical line width tend to be warmer than cores whose line widths are subcritical (JMA).

3.4. IONIZATION AND FIELD-NEUTRAL COUPLING

The low level of ionization in cores is important because it determines how well the core magnetic field can couple to the neutral gas through ion neutral collisions. The ions are essentially tied to magnetic field lines because the period of ion gyration around the field is much shorter than ion-neutral collision times. If the field fluctuates with a period shorter than the time for an ion to hit a neutral, this motion cannot be transmitted to the neutrals, so the field and neutral gas cannot move together as a single-fluid system. This decoupling occurs at the size scale of the MHD cutoff wavelength

$$\lambda_0 = \pi v_A \tau_{in} \tag{7}$$

where v_A is the Alfven speed in the combined system of ions and neutrals, and τ_{in} is the time for an ion to hit a neutral (Kulsrud & Pearce 1969). Such decoupling can limit the cloud's ability to adjust its structure on small scales.

The ionization structure of a molecular cloud is expected to be dominated by ultraviolet (UV) photons from external OB stars in its outer parts, where the visual extinction to the cloud surface is about 4 mag (McKee 1989, Bertoldi & McKee 1992). At higher extinctions, the ionizing flux of UV photons is attenuated below the level of cosmic-ray particles, so cosmic ray ionization dominates. The dominant ion is expected to be HCO^+, arising from ionization of CO.

Attempts to measure the ionization in dense cores have relied on line observations of HCO^+, $H^{13}CO^+$, DCO^+, and $C^{18}O$, and on models of cloud ion-neutral chemical reactions, to estimate the electron fraction x_e (Guelin, Langer & Wilson 1982, Wootten, Loren & Snell 1982). These early studies in a few low-mass cores, led to the estimate that $x_e \approx 10^{-7}$ in cores with density $n \approx 10^4$ cm^{-3}, in close agreement with estimates based on cosmic-ray ionization. More recent studies have cosmic-ray observed several tens of cores, both isolated low-mass cores (Williams et al 1998, Caselli et al 1998) and more massive cores (Bergin et al 1999), and have employed more detailed chemical models. These more recent studies have confirmed the earlier conclusion that core ionization is consistent with simple cosmic-ray ionization, with ionization rates of order 5×10^{-17} s^{-1}.

Figure 7 shows results from the ionization study of 20 low-mass cores by Williams et al (1998), indicating no significant difference in ionization between cores with and without embedded low-luminosity stars.

With these results it follows that the field-neutral coupling in dense cores of radius r is sufficient to allow propagation of MHD waves above their cutoff wavelength. The strength of the coupling is quantified by a

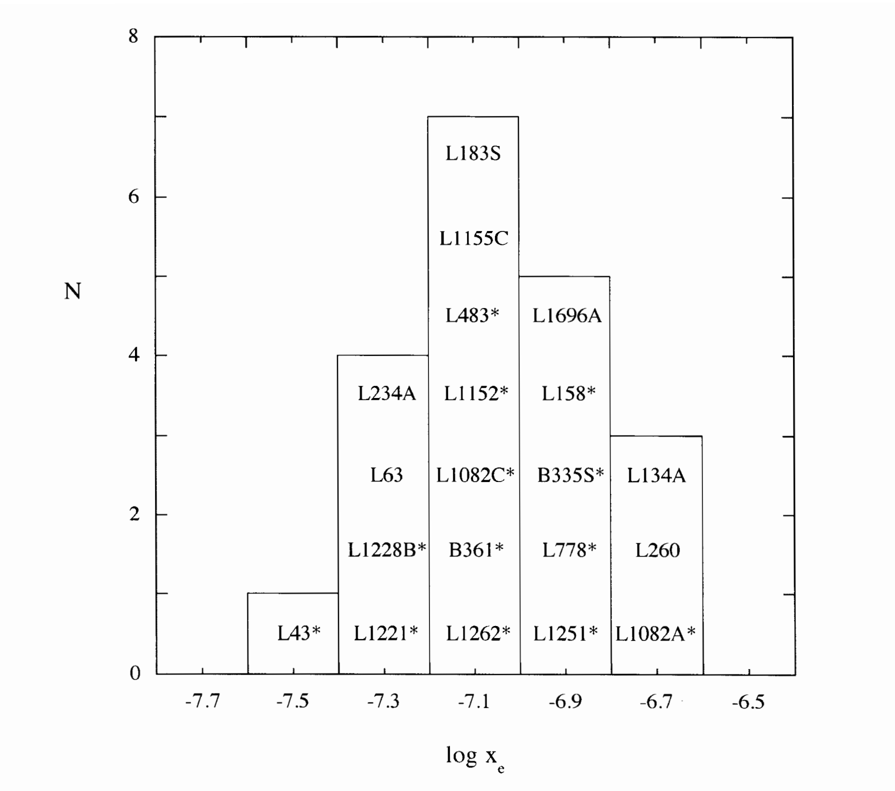

Figure 7. Distribution of electron fraction x_e in 20 low-mass dense cores, based on line observations and chemical models (Williams et al 1998a). Asterisks denote cores with embedded low-mass stars. The distribution peaks at log $x_e \approx$ -7, as expected for ionization dominated by cosmic rays, and shows no significant difference between cores with and without embedded stars.

factor $W \equiv r/\lambda_0$ (Myers & Khersonsky 1995; see also Shu 1983). The foregoing ionization estimates indicate that in the typical dense cores $W \approx 10$. Thus dense cores are not likely to have substantial field-neutral decoupling. However their coupling is significantly weaker than in their surrounding UV-ionized gas, and so they can attenuate externally incident MHD waves (Nakano 1998, Myers & Lazarian 1998).

3.5. LINE WIDTH - SIZE RELATIONS

When cores and their surrounding gas are mapped in tracers such as the lines of NH_3, $C^{18}O$, and ^{13}CO, which are sensitive to a wide range in density, they show a pronounced increase of line width Δv with map size R (Ho et al 1977, Snell 1981, Larson 1981, Fuller & Myers 1992, Caselli & Myers 1995, Barranco & Goodman 1998). This relation is represented as a power law, $\Delta v \sim R^p$, usually with $0.3 < p < 0.7$. This trend is a property of cloud turbulence, since most of the variation in Δv is in its nonthermal, rather than its thermal part. Line width-size relations for many clouds are consistent with hydrostatic equilibrium and with a "logatropic" density structure, in which the density decreases with radius r as r^{-1} (McLaughlin & Pudritz 1996). Many versions of line width-size relation have been described, depending on the number of tracers used and the number of clouds in the sample (Goodman et al 1998a), but in each case the dense core is a local minimum of nonthermal motions, compared to its surrounding gas. A closely related property is the tendency for a low-mass core to be more "coherent" than its surroundings, i. e. for the line widths to show greater uniformity within the core than outside it (Goodman et al 1998b).

In addition to the general properties described above, many aspects of dense cores vary strongly with their level of turbulent motions. For convenience we contast the "thermal" and "turbulent" cores described above as two distinct groups, each represented by cores in Taurus and Orion, respectively.

3.6. ASSOCIATED STARS

Thermal cores tend to have fewer associated stars than do turbulent cores. In Taurus, all of the 20 known NH_3 cores are thermal; about half of these have no associated YSO, and those which have associated YSOs generally have only one. In Orion A and B, nearly all of the 80 known cores are turbulent, only about 10 % are starless, and many are associated with groups and clusters of at least 5 YSOs. This difference in turbulence between Taurus and Orion cores is not simply a consequence of the associated stars and their winds and outflows. Even starless cores in Orion have more turbulence than their Taurus counterparts, and their turbulent line widths are not significantly different from their neighboring cores in Orion having associated stars (JMA). These differences suggest that turbulence is part of the core initial conditions for star formation.

3.7. CORE SIZE

Thermal cores tend to be smaller than turbulent cores by a typical factor of 2. The FWHM diameter of thermal NH_3 cores in Taurus is typically 0.05 pc while the size of the turbulent cores is typically 0.1 pc in Orion (JMA). This result is significant because it means that he volume of gas denser than 10^4 cm^{-3} is about 8 times greater for Orion cores than for Taurus cores. Thus Orion cores have significantly greater mass available to make groups and clusters than do Taurus cores.

3.8. TEMPERATURE

Thermal cores are cooler than turbulent cores: in Taurus the typical temperature is 10 K (Benson & Myers 1989) while in Orion it is more nearly 20 K (Harju, Walmsley & Wouterloot 1993, Cesaroni & Wilson 1996, JMA). This difference in temperature cannot be attributed solely to a greater incidence of stars embedded in the Orion cores, since even starless cores in Orion tend to be substantially warmer than in Taurus. Instead, Orion cores are probably warmer than Taurus cores because they are heated by the much greater number of stars which lie in the Orion complex but outside the cores themselves (JMA).

3.9. EXTERNAL EXCITATION OF CORE TURBULENCE

The similarity of line widths in cores with and without embedded YSOs, and the sharp increase in line width from starless cores not near clusters to those near clusters, together suggest that turbulent cores have substantial external excitation of their turbulence. The environments of Taurus and Orion cores differ in the much greater number of cluster stars outside Orion cores than around Taurus cores, suggesting that the high incidence of winds and outflows from stars around Orion cores helps to maintain the turbulence of Orion cores at a much greater level than is possible for Taurus cores (JMA). For a detailed review of molecular outflows and their environmental effects, see Bachiller (1996) and the chapter in this volumne by Bachiller. A schematic view of external excitation of core turbulence by winds and outflows is shown in Figure 8.

4. Cluster-Forming Cores

The discussion of turbulent cores in Section 3 indicates that star formation in groups and clusters is a major mode of star formation, which may make significantly more stars than the isolated mode. More detailed discussion of cluster observations are in the chapter by E. Lada, and in Lada & Lada (1995). Despite its importance, the clustered mode has been the subject of much less theoretical analysis than the isolated mode, which is well-described by the "standard model" (Shu, Adams & Lizano 1987). In this section we describe recent discussions of clustered star formation.

4.1. MODELS OF CLUSTERED STAR FORMATION

A major goal of clustered star formation models is to account for the characteristic mass ($\sim$1 $M_\odot$) and spacing ($\sim$0.05 - 0.1 pc) of stars observed in young clusters, consistent with the dense core conditions where young

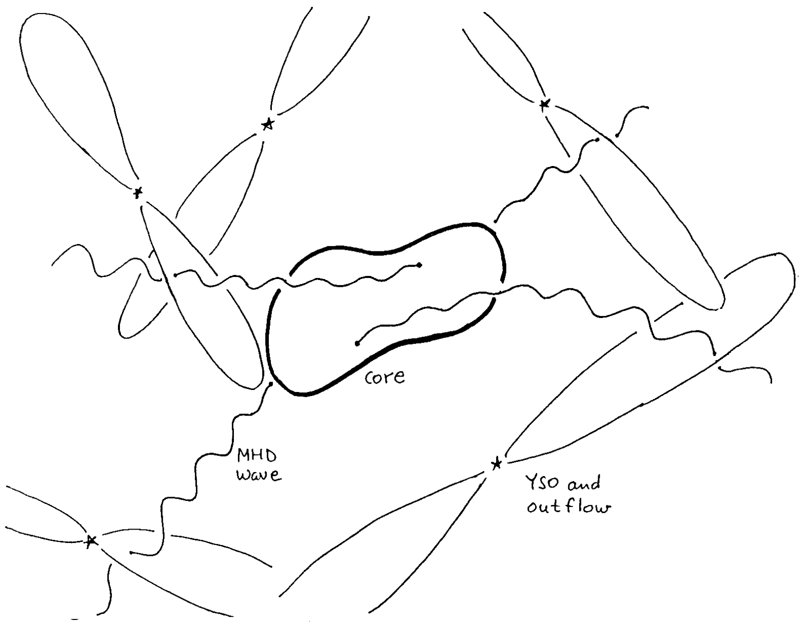

Figure 8. **A schematic illustration of how stars outside a starless core may contribute to core turbulence, through excitation of MHD waves by stellar winds and outflows.**

clusters are found. A second goal is to account for the number distribution of massive stars in clusters, a power-law decrease of the number of stars N with increasing stellar mass M, $dN/dM \sim M^{-p}$, with $p \approx 2$. For a detailed review of this subject, see Larson (1995). Here we describe two easily distinguished pictures of clustered star formation.

The "orbiting seed fragments" model of Bonnell et al (1997) envisions small bound condensations which travel through the gas of the protocluster dense core, accreting mass as they execute many orbits. These fragments compete for mass, somewhat as planetesimals do in models of the solar nebula, resulting in a wide range of masses. The more massive members sink to the densest part of the gravitational potential well, where they accrete mass more rapidly and can collide with each other. This picture accounts for the distribution of stellar masses but not for the particular conditions of dense cores where clusters are found.

The "Jeans mass" models of Larson (1985) and Mouschovias (1991) predict the existence of protostellar condensations with the mass and size needed to match the typical mass and spacing of stars in clusters, but not having the number distribution with mass needed to match the IMF. In these models, self-gravitating condensations form in a medium of fixed

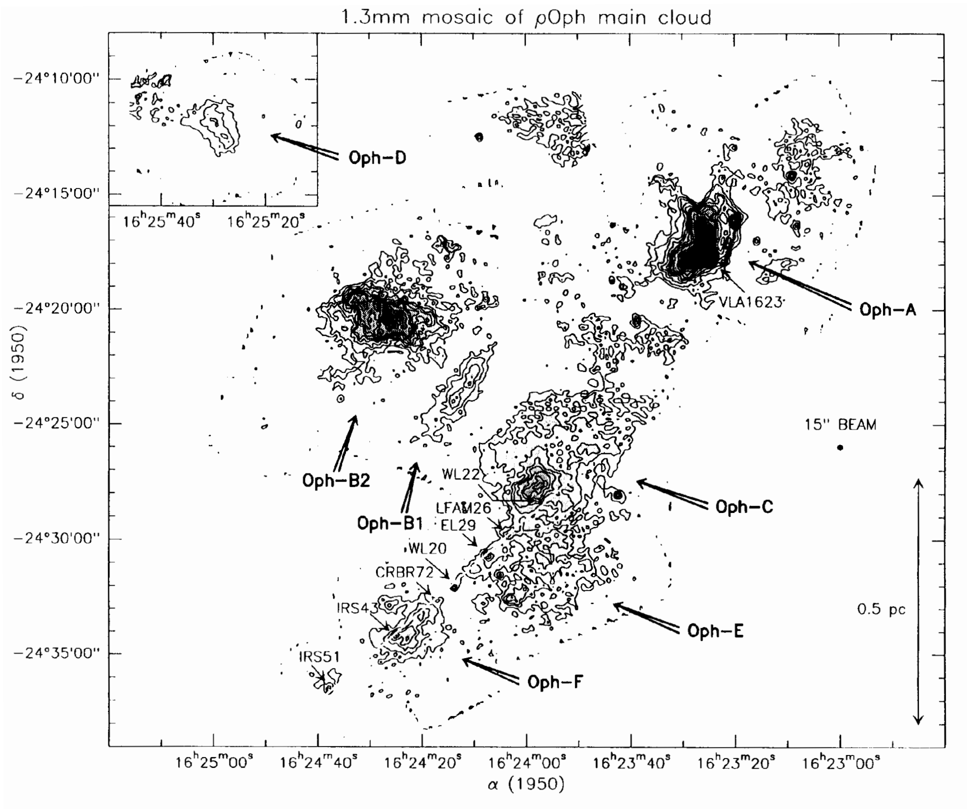

Figure 9. **Emission at 1.3 mm from the L1688 cloud in the Ophiuchus dark cloud complex, showing numerous small condensations associated with the embedded stellar cluster (Motte, Andre & Neri 1998).**

external pressure, as in the Bonnor-Ebert problem (Bonnor 1957, Ebert 1956). In the nonmagnetic case the external pressure is specified by the observed temperature and density (Larson 1985). In the magnetic case the formation of the condensation is motivated by the requirement that the condensation be cut off from external MHD waves (Mouschovias 1991).

4.2. OBSERVATIONAL STUDIES OF YOUNG CLUSTERS

Recent high-resolution observations of young cluster-forming regions show numerous small structures having the spacing and mass distribution expected for cluster members. Motte, Andre & Neri (1998) imaged the Ophiuchus cluster in the 1.3 mm continuum with a bolometer array on the IRAM 30-m telescope, as shown in Figure 9.

Motte et al (1998) found ~50 sources, most of them pointlike, distributed among the young stars known in the cluster region, with about the same projected spacing as the stars. The mass distribution of these objects, although limited by small number statistics, has a slope more similar to that of stars in clusters than to that of interstellar clumps derived from observations of ^{13}CO line emission. A similar result was found in the Serpens cluster by Testi & Sargent (1998), using the OVRO interferometer at 3 mm wavelength. These continuum sources also have spacing consistent with young stars in dense clusters, and have a mass distribution similar to that of the IMF.

4.3. KERNEL MODEL

An extension of the cut-off Jeans mass model, in the context of a turbulent cluster-forming core, was proposed by Myers (1998). In this picture the external pressure is provided by the combination of thermal and MHD turbulent motions thought to account for the observed thermal and non-thermal line widths in cores. In that case a simple estimate indicates that a small condensation within the core - a "kernel" - can exist only when the ratio of Alfven and sound speeds in the surrounding dense core gas is greater than about 3, as illustrated in Figure 10, and when the column density of the core gas is greater than about 10 magnitudes. These conditions add specificity to the Jeans models because they allow precursors of cluster members to form only in the turbulent, high-extinction cores where they are observed, and not in the quiescent, low extinction cores where they are not observed.

A key property of quiescent kernels in turbulent cores is their line width contrast, as shown in Figure 11. A turbulent core with no kernel should have a substantially broader spectral line than would an otherwise identical core with an embedded kernel.

It is desirable to observe the condensations in cluster-forming regions with spectral lines which reveal the condensations' motions in the cloud via their line velocities, and their internal motions via their line widths. Observations of the core "Orion B9" (Caselli & Myers 1995) in the 1-0 line of N_2H^+ with the BIMA interferometer indicates a condensation with HM extent about 0.03 pc, and a line profile with FWHM 0.25 km s-1 – both consistent with expected kernel properties. Observations of the core Oph E mm2d of Motte, Andre & Neri (1998) in the same line with the 30-m telescope indicate a FWHM line width 0.3 km s^{-1} (Motte & Andre 1998). These encouraging observations indicate that it will soon be possible to thoroughly investigate the motions of small condensations in cluster regions, and to test various models of cluster formation.

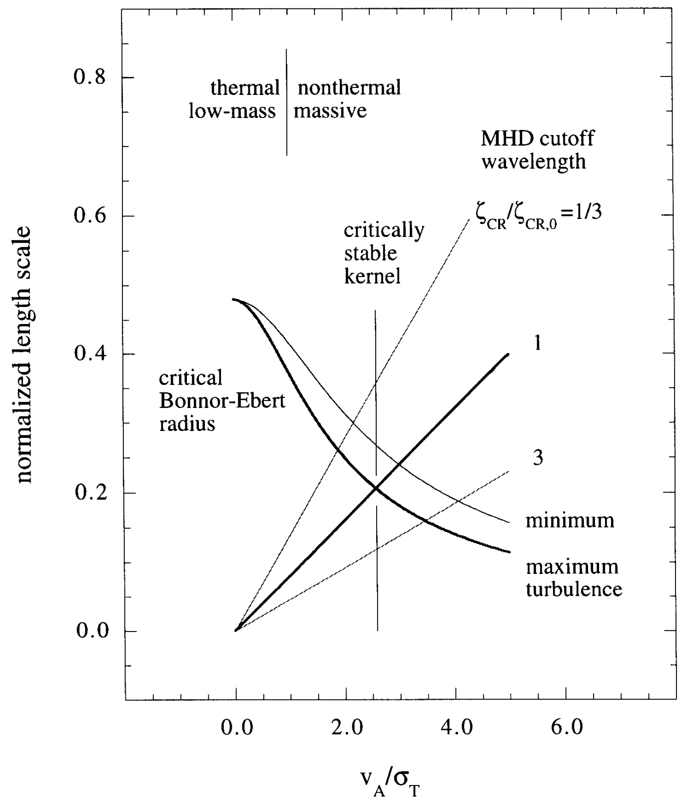

Figure 10. Kernel size scales as a function of Alfven Mach number in the surrounding dense core. The kernel is critically stable when the Bonnor-Ebert radius and MHD cutoff wavelength in the dense core are equal. The size scales, each normalized by the core Jeans length, cross when the Alfven Mach number is $\sim$3, in the regime of massive turbulent cores, as opposed to low-mass, thermal cores (Myers 1998).

5. Inward Motions in Dense Cores

The study of star formation has highly detailed observational knowledge of "initial conditions" and of "young stars" but much less understanding of the physical processes of condensation and collapse which link these two evolutionary states. In the last several years it has become possible to use spectroscopic observations to discern the degree of inward motion in dozens of dense cores with and without associated stars. In this section we briefly review the history, techniques, and recent observations in this area, with emphasis on the earliest phase - the starless cores. More detailed discussion of infall in cores with associated stars is given in the reviews by Myers,

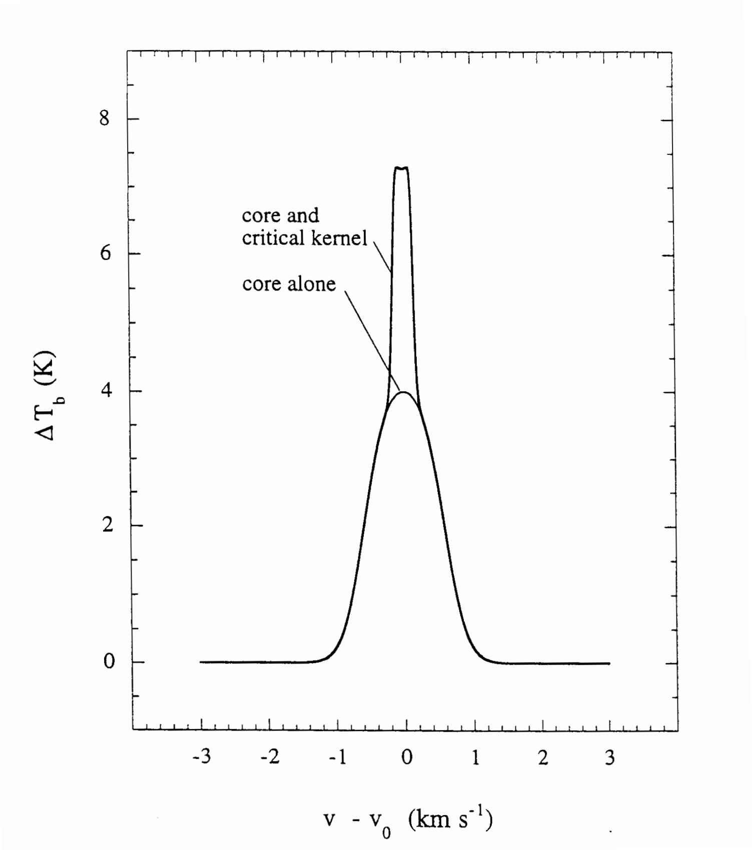

Figure 11. **Predicted profles of emission in the N_2H^+ 1-0 line from a turbulent core with and without a critical kernel (Myers 1998).**

Evans & Ohashi (1999) and by Evans (1999).

5.1. INFALL ASYMMETRY

The basic technique used to infer inward motions in millimeter-wavelength spectral lines is the observation of "infall asymmetry," the skewing of an optically thick spectral line to the blue of an otherwise similar optically thin line. This effect, first explained by Hummer & Rybicki (1968) in the context of lines from expanding H II regions, was used to analyze molecular cloud lines in terms of infall by Lucas (1976), Leung & Liszt (1976), Leung & Brown (1977), and more recently by Walker et al (1986), Adelson & Leung (1988), Zhou (1992), Zhou et al (1993), Walker, Narayanan & Boss (1994), Choi et al (1995), and Myers et al (1996), among others.

Infall asymmetry arises when a foreground region of lower excitation

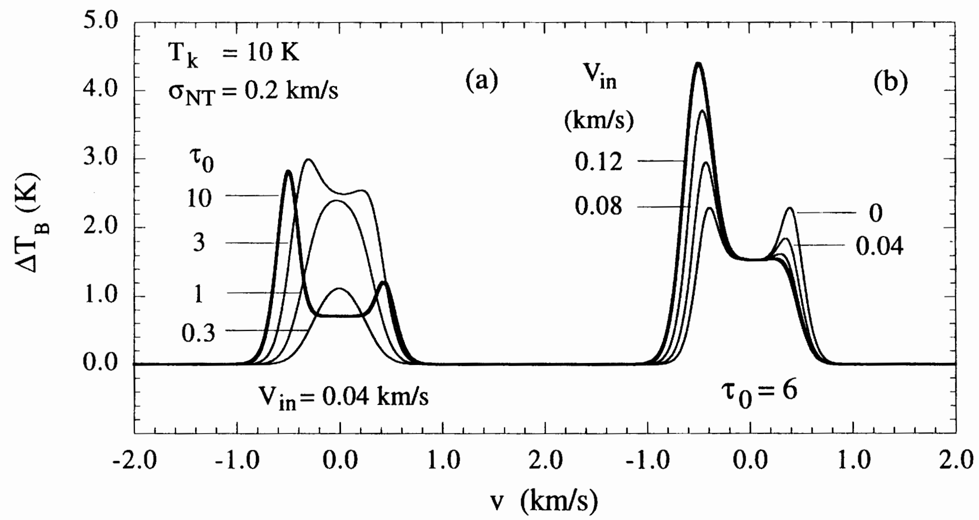

Figure 12. Predicted spectral line profiles from two approaching layers as (a) the peak optical depth increases at fixed approach speed, and (b) the approach speed increases at fixed optical depth. In each case the "infall asymmetry," or skewing of the line profile to the blue, becomes more pronounced (Myers et al 1996).

temperature absorbs photons from a background region of higher excitation temperature, and when the two regions have inward relative motion. The absorption occurs preferentially on the red side of the line profile, yielding a line shape with a peak skewed to the blue, or with a blue peak and a red shoulder, or with two peaks, and with the blue peak brighter than the red peak. The infall asymmetry is evident provided the excitation temperature gradient is sufficiently steep, the foreground optical depth is sufficiently great, and the characteristic infall speed is comparable to the velocity dispersion (Leung & Brown 1979).

The infall asymmetry becomes more pronounced as the optical depth increases, and as the infall speed increases, as illustrated in Figure 12 (Myers et al 1996).

Observation of infall asymmetry has a controversial history, in part because such observation can be taken as evidence of star-forming gravitational infall - a long-sought process of great physical importance. As described in the chapter by Evans, and by Myers, Evans & Ohashi (1998), claims of infall have been challenged or doubted because of confusion by outflows, by inconsistency of infall asymmetry from tracer to tracer, and by a mixture of infall and outflow asymmetry within a map, among other reasons. The climate of opinion began to change with the pioneering work of Zhou et al (1993), who reported infall asymmetry in the dense core B335 containing an extremely red "class 0 protostar" (Andre, Ward-Thompson & Barsony 1993), and who analyzed the observations of CS and H_2CO lines with radiative transfer models based on the "inside-out" collapse model of Shu (1977). Since then the case for infall in cores with embedded candidate protostars has strengthened, through the survey work of Gregersen et al (1997) and Mardones et al (1997).

5.2. INFALL ASYMMETRY IN STARLESS CORES

"Starless" cores are dense cores with no evidence of associated YSOs, based primarily on the IRAS survey (Neugebauer et al 1984) and secondarily on observations, if available, at optical and near- infrared wavelengths. For IRAS observations of the nearest star-forming complexes, lack of detection implies an upper limit on the luminosity of an associated embedded source of about 0.1 $L_\odot$ (Myers et al 1987). Starless cores are also called "pre-protostellar" (Ward-Thompson et al 1994) although it is not clear that every starless core will make a protostar.

The best-studied case of infall asymmetry in a starless core is in L1544, an opaque dark cloud on the eastern edge of the Taurus complex. This core has been mapped at high spectral resolution in lines of CS, H_2CO, C_3H_2, N_2H^+, and $C^{34}S$ (Tafalla et al 1998). It shows infall asymmetry in all of these lines except the optically thin $C^{34}S$ 2-1 line, and the spatial extent of the infall asymmetry appears to increase with the transition optical depth. For example the infall asymmetry extends over 0.02 pc in the N_2H^+ 1-0 line and over 0.15 pc in the CS 2-1 line. The remarkably large extent in CS 2-1 is much greater than the 0.04 pc extent of the HM intensity contour of the N_2H^+ 1-0 emission, often taken as a measure of the extent of the dense core. This pattern of infall asymmetry is shown in Figure 13.

On the smallest scale, the asymmetry in the N_2H^+ 1-0 line has been observed with 10 arcsec resolution using the BIMA interferometer, in combination with data from the IRAM 30-m telescope (Williams et al 1998b). The extent of the asymmetry agrees with the single-dish map, but the combined map shows more spatial detail - an elongated structure with a velocity gradient along the long axis, and with the strongest infall asymmetry at the position where the line is brightest. No continuum point source is evident.

Remarkably, analysis of the line profiles of CS on the large scale and N_2H^+ on the small scale shows about the same characteristic infall speed in each case - about 0.1 km s^{-1}. There is no obvious increase in infall speed with decreasing spatial scale, as would be expected for a strongly centrally condensed source.

The large extent of infall asymmetry in this starless core appears to rule out consistency with the inside-out collapse model of Shu (1977), since an

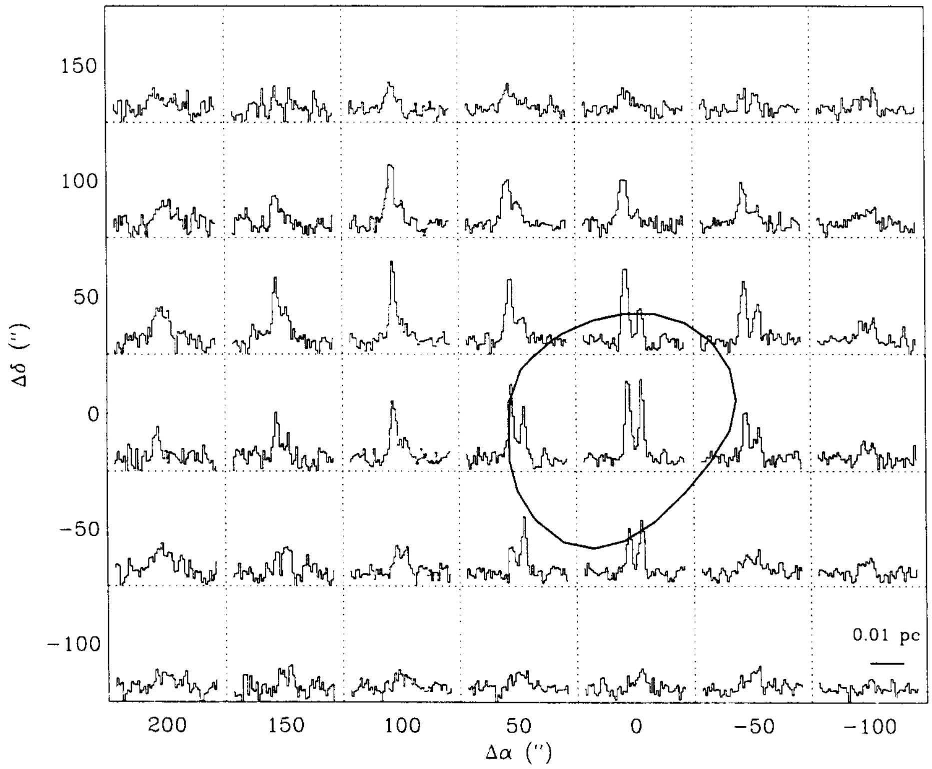

Figure 13. Map of profiles of the CS 2-1 line from the starless core L1544 in relation to the HM contour of the 1-0 line of N_2H^+, a tracer of dense core emission. The CS profiles show infall asymmetry extended over ~0.15 pc, much greater than the extent of the dense core (Tafalla et al 1998).

inside-out collapse of such large radius would have already formed a point source of several $L_\odot$, whereas no protostellar source is known, down to a luminosity limit of about 0.1 $L_\odot$. Similarly, the infall speed appears too fast to match most models of core formation by ambipolar diffusion, which predict infall speeds less than about 0.03 km s^{-1} at the radius and density of observation (e.g., Ciolek & Mouschovias 1995).

The number of starless cores with such spatially extended infall asymmetry is not yet known, but surveys indicate that tens of starless cores show infall asymmetry in at least one tracer (Lee, Myers & Tafalla 1998), and maps indicate asymmetry in CS lines, extended over at least 0.1 pc in L1498 and L429-1 (Lee, Plume & Myers 1998). Evidently spatially extended infall asymmetry in starless cores is not limited to L1544.

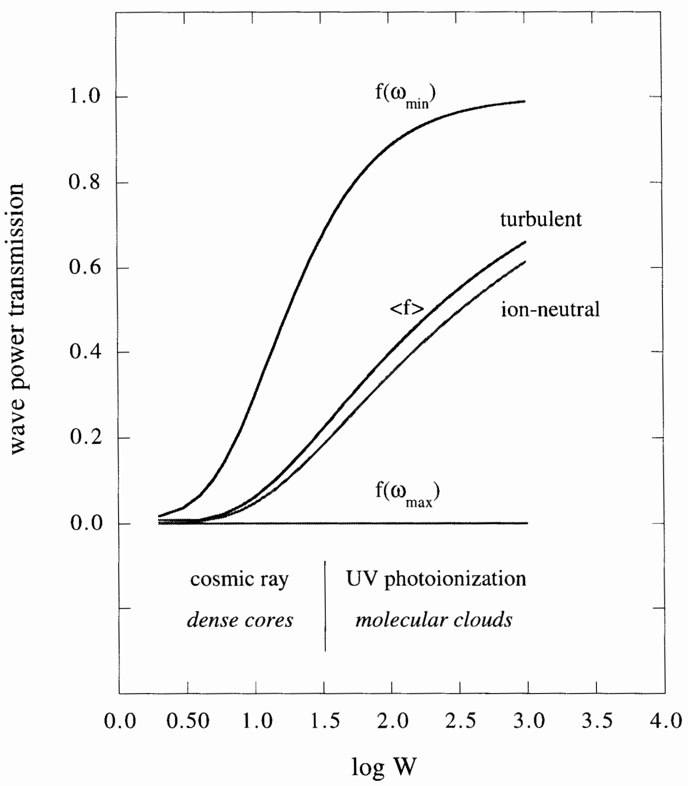

Figure 14. MHD wave power transmission in a region of radius r and MHD cutoff wavelength λ_0, whose ion-neutral friction is described by the coupling parameter $W \equiv r/\lambda_0$. As W decreases from the regime of photoionized molecular cloud to the cosmic-ray-ionized dense core, ion-neutral friction attenuates the MHD waves. This attenuation increases the pressure contrast between the outer and inner regions, driving an inward flow (Myers & Lazarian 1998)

5.3. TURBULENT COOLING FLOWS

In addition to the starless cores described above, some cores with stars also show similarly extended infall asymmetry, including L1251B, Serpens, and NGC 1333 (Mardones et al 1998). These examples suggest that inward motions may in some cases be driven by forces acting on larger scales than expected for gravitational infall. A possible pressure-driven inward flow has been suggested in the context of localized dissipation of turbulent motions (Myers & Khersonsky 1995, Myers & Lazarian 1998).

In this picture, a cooling instability arises as localized dissipation of turbulence decreases the local turbulent pressure, leading to an inward pressure gradient, followed by inward flow along field lines, increasing density, and further dissipation of turbulence. The resulting inward flow is called a "turbulent cooling flow" in rough analogy with cooling flows following thermal cooling in clusters of galaxies (Cowie & Binney 1977).

Figure 14, from Myers & Lazarian (1998), shows that one mechanism of turbulent dissipation, ion-neutral friction, should lead to substantial damping of MHD waves for the level of ionization expected in and near dense cores. This result supports the suggestion of Nakano (1998) that MHD waves and turbulence should soon dissipate following core formation, if no new turbulence is excited, for example by winds from young stars.

The speed of a turbulent cooling flow should be less than the effective speed of the turbulent motions, and estimates for the environments of dense cores indicate that the flow speed has a maximum close to the sound speed, or 0.2 km s^{-1} for a cloud at temperature 10 K (Myers 1998). This suggests that turbulent cooling flows can match the flow speeds indicated by observations of extended infall asymmetry. If so, such flows can condense matter onto dense cores substantially faster than ambipolar diffusion, and can modify and enhance the process of gravitational infall. However more detailed observations and calculations are needed to explore this and other types of pressure-driven flow in molecular clouds.

6. Summary

This chapter reviews physical conditions in nearby molecular clouds, describing basic properties of molecular clouds, dense cores, and their inward motions, in the context of star formation. We focus on the role of turbulence in the support of molecular clouds, in the formation of the precursors of stars in clusters, and in the generation of pressure-driven flows through the dissipation of turbulent motions.

I thank the organizers of the NATO Advanced Study Institute on which this book is based, Charlie Lada and Nick Kylafis, for their invitation and their hospitality, and the other participants for a lively and interesting meeting. Lincoln Greenhill, Judy Lees, and Lee Simmons provided valuable assistance with the figures and with the preparation of the manuscript.

References

Adelson, L. M., & Leung, C. M. 1988, MNRAS, 235, 349
Andre, P., Ward-Thompson, D., & Barsony, M. 1993, ApJ, 406, 122
Bachiller, R. 1996, ARAA, 34, 111
Basu, S., & Mouschovias, T. Ch. 1994, ApJ, 432, 720
Barranco, J. A., & Goodman, A. A. 1998, ApJ, 504, 207
Bell, M. B., Feldman, P. A., Travers, M. J., McCarthy, M. C., Gottlieb, C. A., & Thaddeus, P. 1997, ApJ, 483, L61
Beichman, C. A., Myers, P. C., Emerson, J. P., Harris, S., Matheiu, R., Benson, P. J., & Jennings, R. E. 1986, ApJ, 307, 337

Benson, P. J., & Myers, P. C. 1989, ApJS, 71, 89 Benson, P. J., Myers, P. C., & Wright, E. L. 1984, ApJ, 279, L27
Bergin, E. A., Plume, R., Williams, J. P., & Myers, P. C. 1999, ApJ, in press
Bertoldi, F., & McKee, C. F. 1992, ApJ, 395, 140
Blaauw, A. 1991, in *The Physics of Star Formation and Early Evolution*, eds. C. J. Lada and N. D. Kylafis, Kluwer Acad. Pub., Dordrecht, Netherlands, p. 125
Bonnell, I. A., Bate, M. R., Clarke, C. J., & Pringle, J. E. 1997, MNRAS, 285, 201
Bonnor, W. B. 1956, MNRAS, 116, 351
Caselli, P., & Myers, P. C. 1995, ApJ, 446, 665
Caselli, P., Walmsley, C. M., Terzieva, R., & Herbst, E. 1998, ApJ, 499, 234
Cesaroni, R., & Wilson, T. L. 1994, A&A, 281, 209
Chen, H., Myers, P. C., Ladd, E. F., & Wood, D. O. S. 1995, ApJ, 445, 377
Chen, H., Grenfell, T. G., Myers, P. C., & Hughes, J. D. 1997, ApJ, 478, 295
Choi, M., Evans, N. J., Gregresen, E. M., & Wang, Y. 1995, ApJ, 448, 742
Ciolek, G. E., & Mouschovias, T. Ch. 1995, ApJ, 454, 194
Cowie, L. L., & Binney, J. 1977, ApJ, 215, 723
Ebert, R. 1955, Z. Astrophys., 37, 217
Evans, N. J. 1999, ARAA, 37, in press.
Feige, J., & Pudritz, R. 1998, ApJ, submitted
Fuller, G. A., & Myers, P. C. 1992, ApJ, 384, 523
Fuller, G. A., & Myers, P. C. 1993, ApJ, 418, 273
Goldsmith, P. F., & Langer, W. D. 1978, ApJ, 222, 881
Goodman, A. A., Barranco, J. A., Wilner, D. J., & Heyer, M. H. 1998, ApJ, 504, 223
Gregersen, E., Evans, N. J., Zhou, S., & Choi, M. 1997, ApJ, 484, 256
Guelin, M., Langer, W. D., & Wilson, R. W. 1982, A&A, 107, 107
Harju, J., Walmsley, C. M., & Wouterloot, J. G. 1991, A&A, 245, 643
Harju, J., Walmsley, C. M., & Wouterloot, J. G. 1993, A&AS, 98, 51
Ho, P. T. P., & Townes, C. H. 1983, ARAA, 21, 239
Ho, P. T. P, Martin, R. N., Myers, P C., & Barrett, A. H. 1977, ApJ, 215, L29
Hummer, D. G., & Rybicki, G. B. 1968, ApJ, 153, L107
Jijina, J., Myers, P. C., & Adams, F. C. 1998, ApJ, submitted (JMA)
Kulsrud, R. E., & Pearce, W. P. 1969, ApJ, 156, 445
Lada, C. J. 1999, in *The Physics and Chemistry of the Interstellar Medium*, eds. V. Ossenkopf & J. Stutzki (Aachen: Shaker-Verlag), in press
Lada, E. A., & Lada, C. J. 1995, AJ, 109, 1682
Lada, E. A., Bally, J., & Stark, A. A. 1991, ApJ, 368, 432
Ladd, E. F., Myers, P. C., & Goodman, A. A. 1994, ApJ, 433, 117
Larson, R. B. 1985, MNRAS, 214, 379
Larson, R. B. 1981, MNRAS, 194, 809
Larson, R. B. 1995, MNRAS, 272, 213
Lee, C. W., Myers, P. C., & Tafalla, M. 1998, in preparation
Lee, C. W., Plume, R., & Myers, P. C. 1998, in preparation
Leung, C. M., & Brown, R. B. 1977, ApJ, 214, L73
Leung, C. M., & Liszt, H. S. 1976, ApJ, 208, 732
Li, Z., & Shu, F. H. 1996, ApJ, 472, 211
Linke, R. A., & Goldsmith, P. F. 1980, ApJ, 235, 437
Lizano, S., & Shu, F. H. 1989, ApJ, 342, 370
Lucas, R. 1976, A&A, 46, 473
Maddalena, R. J., Morris, M., Moscowitz, J., & Thaddeus, P. 1986, ApJ, 303, 37
Mardones, D., Myers, P. C., Tafalla, M., Wilner, D. J., Bachiller, R., & Garay, G. 1997, ApJ, 489, 721
Mardones, D., Bachiller, R., Garay, G., Myers, P., Tafalla, M., Wilner, D. J., & Williams, J. P. 1998, in preparation
McLaughlin, D. E., & Pudritz, R. E. 1996, ApJ, 469, 194
McCarthy, M. C., Travers, M. J., Chen, W., Gottlieb, C. A., & Thaddeus, P. 1998, ApJ,

498, L89
McKee, C. F. 1989, ApJ, 345, 782
Mizuno, A., Onishi, T., Yonekura, Y., Nagahama, T., Ogawa, H., & Fukui, Y. 1995, ApJ, 445, L161
Motte, F., Andre, P., & Neri, R. 1998, A&A, 336, 150
Mouschovias, T. Ch. 1991, ApJ, 373, 169
Myers, P. C. 1991, in *Fragmentation of Molecular Clouds and Star Formation*, eds. E. Falgarone, F. Boulanger, & G. Duvert (Dordrecht: Kluwer), p. 221.
Myers, P. C. 1998, ApJ, 496, L109
Myers, P. C., & Benson, P. J. 1983, ApJ, 266, 309
Myers, P. C., & Khersonsky, V. K. 1995, ApJ, 442, 186
Myers, P. C., & Lazarian, A. 1998, ApJ, 507, L157
Myers, P. C., Evans, N. J., & Ohashi, N. 1998, to appear in *Protostars and Planets IV*, eds. V. Mannings, A. Boss, & S. Russell (Tucson: U. of Arizona Press)
Myers, P. C., Fuller, G. A., Mathieu, R. D., Beichman, C. A., Benson, P. J., Schild, R. E., & Emerson, J. P. 1987, ApJ, 319, 340
Myers, P. C., Fuller, G. A., Goodman, A. A., & Benson, P. J. 1991, ApJ, 376, 561
Myers, P. C., Ladd, E. F., & Fuller, G. A. 1991, ApJ, 372, L95
Myers, P. C., Mardones, D., Tafalla, M., Williams, J. P., & Wilner, D. J. 1996, ApJ, 465, L133
Nakano, T. 1998, ApJ, 494, 587
Neugebauer, G. et al 1984, ApJ, 278, L1
Roberge, W. G., & Whittet, D. C. B. 1996, eds., *Polarimetry of the Interstellar Medium*, (San Francisco: ASP Conference Series, v. 97)
Rohlfs, K., & Wilson, T. L. 1996, *Tools of Radio Astronomy* (Berlin: Springer)
Ryden, B. 1996, ApJ, 471, 822
Schilke, P., Groesbeck, T. D., Blake, G. A., & Phillips, T. G. 1997, ApJS, 108, 301
Shu, F. H. 1977, ApJ, 214, 488
Shu, F. H. 1983, ApJ, 273, 202
Shu, F. H., Adams, F. C., & Lizano, S. 1987, ARAA, 25, 23
Snell, R. L. 1981, ApJS, 45, 121
Spitzer, L. 1978, *Physical Processes in the Interstellar Medium* (New York: Wiley), p. 241
Tafalla, M., & Myers, P. C. 1997, ApJ, 491, 653
Tafalla, M., Mardones, D., Myers, P. C., Caselli, P., Bachiller, R., & Benson, P. 1998, ApJ, 504, 900
Testi, L., & Sargent, A. I. 1998, ApJ, 508, L91
Townes, C. H., & Schawlow, A. H. 1975, *Microwave Spectroscopy* (New York: Dover)
Walker, C. K., Lada, C. J., Young, E. T., Maloney, P. R., & Wilking, B. A. 1986, ApJ, 309, L47
Walker, C. K., Narayanan, G., & Boss, A. P. 1994, ApJ, 431, 767
Ward-Thompson, D., Scott, P. F., Hills, R. E., & Andre, P. 1994, MNRAS, 268, 276
Williams, J. P., Bergin, E. A., Caselli, P., Myers, P. C., & Plume, R. 1998a, ApJ, 503, 689
Williams, J. P., Di Francesco, J., Myers, P. C., & Wilner, D. J. 1998b, ApJ, in press
Wood, D. O., Myers, P. C., & Daugherty, D. 1994, ApJS, 95, 45
Wootten, H. A., Loren, R. B., & Snell, R. L. 1982, ApJ, 255, 160
Zhou, S. 1992, ApJ, 394, 204
Zhou, S., Evans, N. J., Kompe, C., & Walmsley, C. M. 1993, ApJ, 404, 232